Micromagnetic modeling of the magnetization dynamics in a circularly exchange-biased and exchange-coupled ferromagnetic multilayer

D. K. Schreiber,[1,2,*] O. G. Heinonen,[3] and A. K. Petford-Long[2]
[1]*Department of Materials Science and Engineering, Northwestern University, 2220 Campus Drive, Evanston, Illinois 60208, USA*
[2]*Materials Science Division, Argonne National Laboratory, 9700 S. Cass Avenue, Argonne, Illinois 60439, USA*
[3]*Seagate Technology, Bloomington, Minnesota 55435, USA*
(Received 26 March 2009; revised manuscript received 8 June 2009; published 8 July 2009)

The magnetization dynamics of a magnetically coupled multilayer structure have been studied by analytical and numerical methods. The simulated multilayer is disk-shaped and consists of a circularly exchange-biased ferromagnetic permalloy (Py) layer coupled to an unbiased Py layer, each in a magnetic vortex configuration, separated by a thin nonmagnetic spacer. The sign and strength of the interlayer exchange coupling was varied, leading to either parallel or antiparallel vortex chiralities in the two Py layers. The magnetization dynamics after the application of an external magnetic field pulse normal to the plane of the disks were investigated. Both analytical and numerical models show two branches of frequency response of circularly symmetric eigenmodes for both parallel and antiparallel configurations. However, the upper branch mode in the antiparallel configuration is severely damped in the numerical simulations due to coupling with short-wavelength spin waves. The frequency of the modes can be tuned independently with interlayer exchange coupling strength and exchange-bias strength. The good agreement between the mode frequencies obtained from the analytical and numerical models confirms that the main driving forces for the eigenmodes are the magnetostatic field from the radial motion of the magnetization, and also the interlayer exchange coupling field. In addition, the vortex cores, which are neglected in the analytical model, are found to play no significant role in the dynamic response.

DOI: 10.1103/PhysRevB.80.014411 PACS number(s): 75.40.Gb, 75.30.Et, 75.75.+a, 76.50.+g

I. INTRODUCTION

A magnetic vortex is the stable magnetic configuration for micron-sized, nanometer-thick ferromagnetic (FM) disks.[1] In a magnetic vortex, the magnetization lies in the plane of the disk in a flux-closure configuration, with a central core at which the magnetization is perpendicular to the plane of the disk.[2] The vortex can be described by the sense of magnetic circulation (chirality) and by the orientation of the central core (polarity). The chirality and polarity are independent of each other, and can be used to define four unique magnetic configurations. The presence of a vortex affects both the quasistatic[3] and the dynamic[4] response of the magnetization to applied magnetic fields. In the quasistatic response, an external magnetic field applied in the plane of the disk causes a lateral displacement of the vortex core perpendicular to the applied field direction as the magnetic moments align with the field. The presence of the magnetic vortex also plays an important role in the dynamic response of the magnetization to a magnetic field. This is the case both for the relatively low-frequency gyrotropic mode,[5–7] in which the vortex core is displaced and then precesses back to its equilibrium position, as well as for high-frequency eigenmodes[8] that can be excited by in-plane and out-of-plane magnetic field pulses.

These eigenmodes can be described by a set of integers (n,m) which define the symmetry and order of the excited mode. Here, $n>0$ represents the number of nodes in the radial direction at a fixed azimuthal angle, while $2|m|$ denotes the number of nodes in the azimuthal direction at a fixed radial position. When the vortex is excited by an out-of-plane magnetic field pulse, the resulting eigenmodes are circularly symmetric and $m=0$ as there are no azimuthal nodes. However, when excited by an in-plane magnetic field pulse, the circular symmetry is broken and eigenmodes with $m\neq 0$ are excited. Recent advancements in ultrafast, time-resolved magnetic imaging techniques based on the magneto-optical Kerr effect (MOKE) and photoemission electron microscopy (PEEM) have allowed the experimental visualization of both the circularly symmetric[9] $(n,m=0)$ and azimuthal $(n,|m|>0)$ modes[10] excited by out-of-plane and in-plane magnetic field pulses, respectively, in patterned ferromagnetic disks.

Previous studies of the magnetization dynamics of magnetic vortices have focused on single layer[9] or exchange-biased bilayer[11] FM disks. However, to date there has been relatively little work on the dynamics in magnetic heterostructures consisting of two FM disks separated by a thin, nonmagnetic layer. In this trilayer configuration, the magnetostatic and exchange interactions between the two FM disks can alter the remanent state and also the quasistatic and dynamic behavior of the FM layers. These magnetic interactions potentially offer added degrees of control over the dynamic and quasistatic behavior of the magnetization, compared with single-layer or bilayer vortex configurations. In addition, this structure is of practical significance as it is capable of showing giant magnetoresistance (GMR) or tunneling magnetoresistance with the proper choice of ferromagnetic and spacer materials and dimensions, which could potentially be exploited in future magnetic random access memory technologies.[12]

Buchanan *et al.*[13] have reported on the stable remanent magnetization states of a magnetic disk-shaped trilayer structure consisting of two permalloy (Py) layers separated by a

Cu spacer of 1–20 nm thickness. Each Py layer had a diameter of 1.2–2.5 μm and thickness 20–40 nm. From micromagnetic simulations, they found that when a vortex configuration is energetically preferred, the chirality of the vortices in the two disks can be either parallel or antiparallel as the spacer thickness and the sign and strength of the interlayer exchange coupling (IEC) field between the two disks is varied. Increasing the strength of the IEC was found to help stabilize a remanent double-vortex structure over the single-domain structure. Guslienko *et al.*[14] have also reported on the low-frequency coupled gyrotropic response of magnetization to an in-plane magnetic field in the antiparallel trilayer configuration. More recently, Montoncello *et al.*[15] have presented results from micromagnetic simulations of a disk-shaped (200 nm diameter), asymmetric trilayer structure consisting of two Py layers, 10 and 20 nm thick, respectively, separated by a 10 nm nonmagnetic spacer. In this work, the authors report on the high-frequency dynamics of the two ferromagnetic layers, and found a splitting of the frequency response of the expected eigenmodes in the layers into an in-phase and an out-of-phase response, with the frequency difference between the two branches decreasing with increasing mode number. Due to the presence of the thick (10 nm) nonmagnetic spacer layer, the dynamics were driven primarily by magnetostatic interactions between the two layers and interlayer exchange coupling between the two Py layers was not discussed.

Interlayer exchange coupling between two ferromagnetic thin films across a thin nonmagnetic spacer has been used for many years in magnetic field sensor technology as a means of setting the relative orientation of magnetization within the ferromagnetic layers, for example in those used in magnetic field sensors based on giant magnetoresistance.[16,17] IEC has also been used in spin-valves in the so-called synthetic antiferromagnetic trilayer in order to control the magnetostatic fields in the GMR stack.[18] In addition to IEC interactions across metal spacers, both positive and negative IEC have also been observed across oxide spacers such as MgO.[19,20] Exchange bias of a ferromagnetic thin film by an adjacent antiferromagnetic (AF) layer, such as IrMn, has also been used to control the magnetization in data storage structures. While linear exchange bias has been used for many years in data storage technologies, Sort *et al.*[21] have recently demonstrated that a circular exchange bias can be obtained in patterned Py/IrMn bilayers with a vortex remanent state. This is accomplished by heating the bilayer to a temperature above and subsequently cooling back below the blocking temperature of the AF IrMn layer, but always remaining below the Curie temperature of the Py layer. In this way, the magnetization of the AF layer is set by the stray fields of the Py layer, which is in a vortex configuration. Tanase *et al.*[3] have experimentally demonstrated that such a treatment can affect the quasistatic behavior and vortex annihilation/nucleation behavior of Py/IrMn and CoFe/IrMn bilayers. In addition, micromagnetic simulations have demonstrated that this circular exchange bias also affects the dynamic response of the vortex[5,11] in both the gyrotropic and spin-wave frequency regimes by changing the energy potential of the vortex. In general, interlayer exchange coupling and exchange bias are two avenues to controlling the remanent, quasistatic, and dynamic behavior of the magnetization in a patterned ferromagnetic structure.

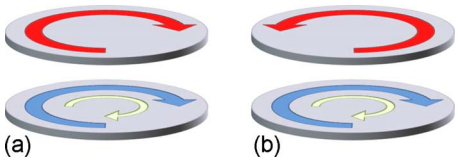

FIG. 1. (Color online) Energetically allowable magnetic configurations for (a) positive and (b) negative interlayer exchange coupling between the two disks. The white arrow indicates the direction of the exchange-bias field in the PL, while the blue and red arrows indicate the chirality of the vortex in the PL (bottom) and FL (top), respectively.

In this work, the coupled high-frequency eigenmodes excited by a magnetic field pulse normal to the plane of a magnetic heterostructure are investigated by a simple analytical model and by dynamical micromagnetic simulations. In particular, the (1,0)-type eigenmodes of the system are considered. The simulated heterostructure consists of two ferromagnetic layers of Py separated by a thin, nonmagnetic spacer layer. The magnetization in both Py layers is set in a vortex configuration, with either parallel or antiparallel vortex chirality, and one Py layer experiences a circular exchange-bias field from an adjacent antiferromagnetic layer of IrMn as discussed in detail in a later section. In particular, the ability of the interlayer exchange coupling field between the two ferromagnetic layers and the exchange-bias field from the AF layer to control the dynamic magnetic behavior and frequency of the (1,0)-type modes are considered in detail.

II. ANALYTICAL MODEL AND NUMERICAL SIMULATION DETAILS

The magnetic heterostructure under consideration in this study was set up to simulate an exchange-biased magnetic junction, consisting of an AF layer and two FM layers separated by a nonmagnetic spacer. The spacer can be either an insulator, such as MgO for the case of magnetic tunnel junctions, or a metal, such as Cu for the case of a current-perpendicular-to-plane spin valve structure. The FM layers were both simulated to be Py. Each FM layer was disk-shaped with a diameter of 1 μm and 12 nm thickness, for which the lowest energy magnetic configuration within each layer is a vortex. The ferromagnetic exchange coupling between the two FM layers was set to zero, and instead, the two FM layers interacted via an interlayer exchange coupling field whose strength could be varied to simulate, for example, the spacer thickness or composition.[19,20] An AF pinning layer was simulated by defining an exchange-bias field, the strength of which was chosen to be consistent with IrMn, and which exerted a circular exchange bias on one of the FM layers, which will be referred to as the pinned layer (PL). The second FM layer experienced no exchange bias from the AF layer and will be referred to as the free layer (FL). Two equilibrium magnetic configurations were identified dependent upon the sign of the interlayer exchange coupling be-

tween the two FM layers, as shown in Fig. 1. When the IEC is positive, the two FM layers share a common vortex chirality, while a negative IEC will lead to an antiparallel vortex chirality. Both analytical and numerical models were used to study the coupled dynamic magnetic response of the lowest-order eigenmodes excited by a magnetic field applied normal to the layers.

A. Analytical calculations

In order to gain some understanding for how the lowest-order eigenmodes interact through interlayer exchange coupling and magnetostatic fields, a simple variational analytical model was considered for the lowest-order eigenmodes and the response of the system to an out-of-plane ac magnetic field. This model described two circular disks, each of radius R, thickness d, and magnetization density M_S. The separation between the disks was assumed to be negligible, and the magnetization in each disk was uniform along the z axis, which was perpendicular to the plane of the disks. One of the FM layers (PL), was in contact with an antiferromagnet and subjected to an exchange-bias field $\boldsymbol{H}_{\mathrm{eb}}=H_{\mathrm{eb}}\hat{\varphi}$, and the magnetization of both layers was taken to be in an equilibrium vortex configuration with the same or opposite chirality in the two layers, depending on the sign of the IEC. The two layers interact through an effective interlayer exchange coupling field, H_{IEC}, arising because of interlayer exchange coupling, such as Néel orange peel coupling[22] or interlayer Ruderman-Kittel-Kasuya-Yosida interactions.[23] Linear perturbations were considered about the equilibrium configurations shown in Fig. 1 with the assumptions that the vortex cores could be neglected and that the magnetization excitations in each layer were dominated by the (1,0) eigenmodes. The radial part of these eigenmodes was taken to be $J_1(k_R r)$, with $x=k_1 R$ the first zero of $J_1(x)$, and these were taken to be approximate eigenfunctions[8,9] of the radial component of the magnetostatic field operator $\hat{h}_r[\boldsymbol{M}(\boldsymbol{r})]$. These trial functions satisfy the boundary condition of vanishing radial eigenmode on the edge of the disk. Finally, it was assumed that the magnetostatic field in the z direction due to perturbations of the magnetization in layer $i=1$, 2, corresponding to the PL and the FL, did not extend outside layer i (this was based on the assumption that the magnetization density was uniform along the z axis, and that the thickness of the layers was very small).

The dynamics were described by the coupled Landau-Lifshitz-Gilbert (LLG) equations,

$$\frac{d\boldsymbol{m}_i}{dt}=-\frac{\gamma_e}{1+\alpha^2}[\boldsymbol{m}_i\times\boldsymbol{H}_i]-\frac{\gamma_e\alpha}{1+\alpha^2}\boldsymbol{m}_i\times[\boldsymbol{m}_i\times\boldsymbol{H}_i], \quad (1)$$

where $\boldsymbol{m}_i(\boldsymbol{r})=\boldsymbol{M}_i(\boldsymbol{r})/M_S$, $i=1$, 2, and α is the dimensionless damping constant; $\boldsymbol{H}_i(\boldsymbol{r})$ are the effective fields, including an out-of-plane ac field $H_{ext}e^{-i\omega t}\hat{z}$ acting on layer i. The electron gyromagnetic factor is given by γ_e and the cgs system of units is used. The spatial and temporal dependence of the magnetizations and fields are implied and are not written out explicitly for ease of notation. Ignoring initial transients, the time dependence of all fields and magnetizations are then given by $e^{-i\omega t}$ in a linear-response approximation. An out-of-plane ac field only excites modes that are circularly symmetric, given the circularly symmetric equilibrium states. The magnetization directors were linearized about the equilibrium configurations,

$$\boldsymbol{m}_1=\hat{\varphi}+m_{1r}\hat{r}+m_{1z}\hat{z},$$

$$\boldsymbol{m}_2=\varepsilon\hat{\varphi}+m_{2r}\hat{r}+m_{2z}\hat{z}, \quad (2)$$

where $\varepsilon=\pm 1$. The effective fields are

$$\boldsymbol{H}_1=H_{\mathrm{IEC}}\boldsymbol{m}_2-4\pi M_S m_{1z}\hat{z}+H_{\mathrm{eb}}\hat{\varphi}-M_S N_r m_{1r}\hat{r}-M_S N_r m_{2r}\hat{r}+H_{ext}\hat{z},$$

$$\boldsymbol{H}_2=H_{\mathrm{IEC}}\boldsymbol{m}_1-4\pi M_S m_{2z}\hat{z}-M_S N_r m_{2r}\hat{r}-M_S N_r m_{1r}\hat{r}+H_{ext}\hat{z}, \quad (3)$$

with $\hat{h}_r[m_{ir}(\boldsymbol{r})]=-M_S N_r m_{ir}\hat{r}$. Upon linearizing Eq. (3), we obtain

$$\frac{d}{dt}\begin{pmatrix}m_{1r}\\ m_{1z}\\ m_{2r}\\ m_{2z}\end{pmatrix}=\frac{\gamma}{1+\alpha^2}\begin{pmatrix}-\alpha(\varepsilon H_{\mathrm{IEC}}-M_S N_r+H_{\mathrm{eb}}) & (H_d+H_{\mathrm{eb}}+\varepsilon H_{\mathrm{IEC}}) & \alpha(H_{\mathrm{IEC}}+M_S N_r) & -H_{\mathrm{IEC}}\\ -(M_S N_r+\varepsilon H_{\mathrm{IEC}}+H_{\mathrm{eb}}) & -\alpha(\varepsilon H_{\mathrm{IEC}}-H_d+H_{\mathrm{eb}}) & -(M_S N_r-H_{\mathrm{IEC}}) & \alpha H_{\mathrm{IEC}}\\ \alpha(H_{\mathrm{IEC}}+M_S N_r) & -\varepsilon H_{\mathrm{IEC}} & \alpha(M_S N_r-\varepsilon H_{\mathrm{IEC}}) & \varepsilon H_d+H_{\mathrm{IEC}}\\ -(\varepsilon M_S N_r-\varepsilon H_{\mathrm{IEC}}) & \varepsilon H_{\mathrm{IEC}} & -(\varepsilon M_S N_r+H_{\mathrm{IEC}}) & -\alpha(\varepsilon H_{\mathrm{IEC}}-H_d)\end{pmatrix}\begin{pmatrix}m_{1r}\\ m_{1z}\\ m_{2r}\\ m_{2z}\end{pmatrix}+\frac{\gamma}{1+\alpha^2}\begin{pmatrix}-H_{ext}\\ \alpha H_{ext}\\ -H_{ext}\\ \alpha H_{ext}\end{pmatrix}\begin{pmatrix}m_{1r}\\ m_{1z}\\ m_{2r}\\ m_{2z}\end{pmatrix}, \quad (4)$$

where $H_d=4\pi M_S$, which can then be solved for the two stable magnetic configurations illustrated in Fig. 1.

B. Numerical micromagnetic simulation details

Numerical simulations based on the Landau-Lifshitz-Gilbert equation of motion were conducted to verify that the assumptions used within the analytical calculations are valid. The main assumptions in the analytical model were: core-core interactions between the two disks were neglected, higher-order eigenmodes were neglected, and the stability of the magnetic configuration used within the model.

The magnetization dynamics were simulated by integrating the LLG equation of motion, Eq. (1), using a Bulirsch-Stör integrator optimized for the LLG equation with adaptive step size and error control.[24] The effective field is now given by $\boldsymbol{H}_{eff}=\boldsymbol{H}_{ex}+\boldsymbol{H}_d+\boldsymbol{H}_a+\boldsymbol{H}_{\mathrm{eb}}+\boldsymbol{H}_{\mathrm{IEC}}$. Here,

$$\boldsymbol{H}_{ex}=M_S\delta^2\nabla^2\boldsymbol{m} \tag{5}$$

is the contribution from the ferromagnetic exchange, with $\delta^2=2A/M_S^2$, and A is the exchange coupling in units of energy per unit length. The magnetostatic field $\boldsymbol{H}_d$ is

$$\boldsymbol{H}_d(r)=-\int\frac{d\boldsymbol{r}'(\boldsymbol{r}-\boldsymbol{r}')\nabla'\cdot\boldsymbol{M}_S(\boldsymbol{r}')}{|\boldsymbol{r}-\boldsymbol{r}'|^3}; \tag{6}$$

and the anisotropy field

$$\boldsymbol{H}_a=\frac{2K_u\boldsymbol{m}(r)[\boldsymbol{m}(r)\cdot\boldsymbol{n}(r)]}{M_S} \tag{7}$$

arises from a uniaxial energy density of magnitude K_u and director $\boldsymbol{n}(\boldsymbol{r})$. The heterostructure was simulated as two Py layers with a negligible space between them. The interlayer exchange coupling between the two ferromagnetic layers was taken as $\boldsymbol{H}_{\mathrm{IEC},i}=H_{\mathrm{IEC}}\boldsymbol{m}_j$ where $\boldsymbol{m}_j$ is the magnetization director on the surface of layer j adjacent to layer i. Finally, $\boldsymbol{H}_{\mathrm{eb}}(\boldsymbol{r})$ is the effective field resulting from the exchange bias from the antiferromagnetic layer adjacent to the PL. In terms of cell size a, the magnitude of this effective field is $H_{\mathrm{eb}}=\varepsilon_{\mathrm{eb}}/(M_S a)$ where $\varepsilon_{\mathrm{eb}}$ is the exchange-bias energy in units of erg/cm^2. Cubic cells with edge lengths of either 2 or 4 nm were used. No discernible differences were seen as a result of change in grid size. Numerical values appropriate for Py were used, with $A=1.0\times10^{-6}$ erg/cm and $M_S=800$ emu/cm^3. A uniaxial anisotropy field of $H_a=5$ Oe was applied along the x axis.

In order to study the dynamic behavior of the system, an external magnetic field was applied along the z axis and the system was equilibrated for 3–10 ns in this field. The field was then removed, and the LLG equation was integrated for 4–10 ns and the magnetization density was saved every 0.02 ns. The maximum allowed error over all magnetization directors was set at 1 μrad, and the maximum angular excursion during each time step was limited to 10°. These values ensure robust integration for these systems. The magnetization was averaged across each disk individually, and temporal fast Fourier transforms (FFTs) were taken of both the averaged values of m_z and m_r for both the pinned and free layers. A Fourier transform method[25] was used to image the response at each FFT peak in order to confirm the symmetry of the mode. For some configurations the magnetization response to an ac driving field was also calculated for a range of fixed frequencies.

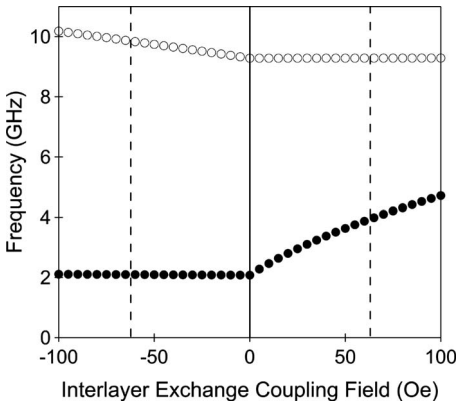

FIG. 2. Analytically calculated resonant frequencies of the (1,0) coupled modes as a function of IEC for $H_{\mathrm{eb}}=104$ Oe. The plot shows two branches of response for both positive and negative values of IEC. The upper branch for negative IEC and lower branch for positive IEC vary strongly with IEC, while the other two branches are relatively unaffected by IEC field. The vertical dashed lines at ±60 Oe denote the IEC values used for more detailed investigations.

III. RESULTS

Numerical simulations were first used to confirm the expected stable magnetic configurations illustrated in Fig. 1. The magnetization of the two disks was initiated in a vortex configuration following the schematics shown in Fig. 1 and then allowed to equilibrate for 10 ns. The stable magnetic configuration for zero or positive values of IEC was found to be that of parallel vortex chirality and core polarity both in zero field and after equilibration in a 100 Oe field applied normal to the plane of the disks [Fig. 1(a)]. For negative values of IEC, the stable magnetic configuration was again a vortex in both disks, with opposite chirality but parallel core polarity [Fig. 1(b)]. The two vortex cores were found to lie directly above each other for both positive and negative values of IEC. Note that in both cases the exchange bias from the AF layer was fixed, which also fixed the chirality of the first FM layer in one particular direction.

The linearized equations of motion arising from the analytical model were solved for the two stable magnetic configurations shown in Fig. 1. Note that for $\varepsilon=1$, $H_{\mathrm{IEC}}>0$, and for $\varepsilon=-1$, $H_{\mathrm{IEC}}<0$, within the analytical model. The resulting solution of the coupled (1,0) eigenmodes showed two branches as the interlayer exchange coupling field was varied, as seen in Fig. 2. For negative values of IEC, the two modes varied slowly with changing IEC strength, with the lower branch showing almost no change in its resonant frequency. In contrast, for positive IEC the frequency of the lower branch increases very quickly with IEC strength. However the upper branch for positive IEC again shows very little change with IEC.

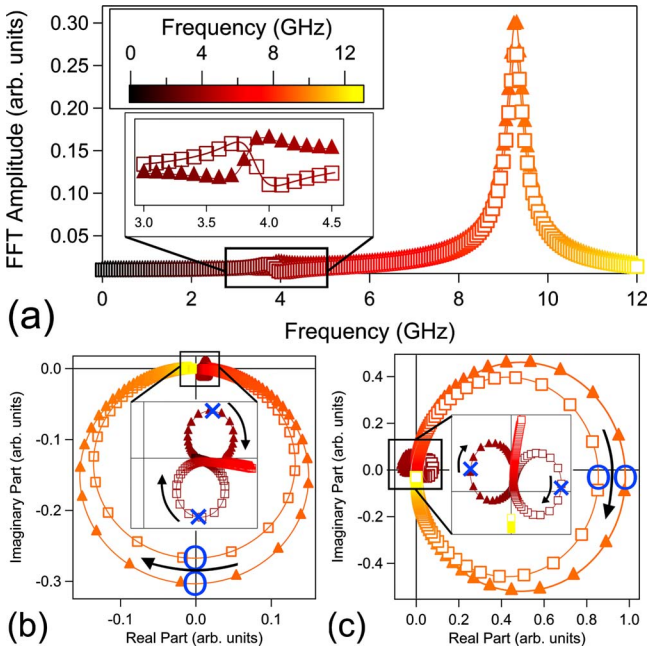

FIG. 3. (Color online) (a) FFT spectra of the m_z component response to an ac magnetic field in the PL (▲) and FL (□) for H_{IEC}=+60 Oe, H_{eb}=100 Oe, calculated from the analytical model. Two modes are present at 9.3 and 3.9 GHz (magnified in inset). The figure is redrawn on an Argand plot (b) to better visualize the phase relation between the PL and FL at both frequencies and the m_r-component response is also plotted (c). The frequency is plotted on a thermal scale shown in (a) and the peak frequencies positions are highlighted with a (◯) and (×) for the upper and lower branches respectively. Arrows are included to indicate the direction of increasing frequency. At the lower frequency, the m_r components in the PL and FL move ~180° out of phase, as do the m_z components. At the high-frequency mode both components move in phase.

A more detailed investigation of the two branches was conducted for two cases: H_{IEC}=+60 Oe and H_{IEC}=−60 Oe. In both instances H_{eb}=100 Oe. These two values of IEC are highlighted by vertical dashed lines in Fig. 2, and correspond to the two magnetic configurations shown in Figs. 1(a) and 1(b). Both the analytical and numerical models were used to study these two systems in detail. In the analytical model, an ac driving field was applied to the system in order to extract the susceptibility and linear response as functions of frequency of the driving field. The following sections discuss the behavior of the upper and lower branches for the case of positive and negative IEC in greater detail. It should be noted that for technical simplicity in the numerical simulations, the IEC field values were H_{IEC}=+62.5 Oe and H_{IEC}=−62.5 Oe. The dispersion relation seen in Fig. 2 shows that a 2.5 Oe offset causes only an inconsequential shift in the frequency within the analytical model.

A. Dynamic response for positive interlayer exchange coupling

The analytical model was first used to investigate the dynamic response for positive IEC. The frequency response of the m_z component of magnetization of each FM layer to an applied ac magnetic field is plotted in Fig. 3(a) for H_{IEC} =60 Oe and H_{eb}=100 Oe. In this figure, the frequency is color-coded from black to yellow with increasing frequency from 0 to 13 GHz. The two branches of the solution are readily seen as two distinct peaks for each layer. The high-frequency peak appears well defined for both the free and pinned layers at 9.3 GHz, with the PL showing a stronger response than the FL. The shape of the low-frequency mode [inset of Fig. 3(a)], at a frequency of about 3.9 GHz, is clearly different from the high-frequency peak, and its nature is not easy to ascertain from the amplitude-frequency plot.

In order to understand the amplitudes and relative phase of the response in the two layers, Argand diagrams of the real and imaginary components of the response were constructed for both layers, and are shown in Fig. 3(b). The frequency of each data point is displayed using the same color-coding as used in Fig. 3(a), and small arrows are included in each Argand diagram to indicate the direction of increasing frequency. The frequency of the modes can be determined from the points at which the curves are at extrema from the zero-frequency point, and are indicated in the figure as (×) and (◯) for the lower and upper branches, respectively. From the Argand diagram, it can be seen that the response of m_z for the pinned layer and the free layer are 180° out of phase and have small amplitude at the low-frequency mode [inset of Fig. 3(b)]. In contrast, the responses of m_z for the two layers at the high-frequency mode are in phase and have large amplitude. Similar Argand diagrams, showing the response of the radial components of magnetization, m_r, for the PL and FL are depicted in Fig. 3(c). This figure shows that the responses of m_r for the PL and FL are 180° out of phase and have small amplitude at the low-frequency mode, whereas at the high-frequency mode the responses of the two FM layers are in phase and have large amplitude. Together, these two Argand plots show that at the low-frequency mode, both the radial and z components of the magnetization in the two FM layers act ~180° out of phase relative to each other, while for the high-frequency mode the magnetization in the two layers moves in phase. In addition, the radial components of the magnetization are 90° out of phase relative to the z components. Finally, the response of the magnetization in the PL is of larger amplitude than that of the FL for the high-frequency mode, whereas the converse is true for the low-frequency mode.

For the numerical simulations, temporal FFTs were calculated from the average values of the m_z and m_r components of magnetization for each ferromagnetic layer. The results were then plotted on Argand diagrams similar to those used for the analytical mode, and are shown in Figs. 4(a) and 4(b). The plots share a number of similar features with their analytical counterparts shown in Figs. 3(b) and 3(c). Both plots show two circular traces, from which the mode frequencies can be determined as approximately 3.5 and 6.0 GHz. Similar to the results from the analytical model, for both m_r and m_z the low-frequency responses of the FL and PL are out of phase, while they are in phase at the high-frequency mode. The frequency obtained for the lower mode from the analytical and numerical models is in very good agreement, while there is a larger discrepancy for the upper mode. This is because the upper mode is driven primarily by the magnetostatic fields, which are less accurately represented by the trial

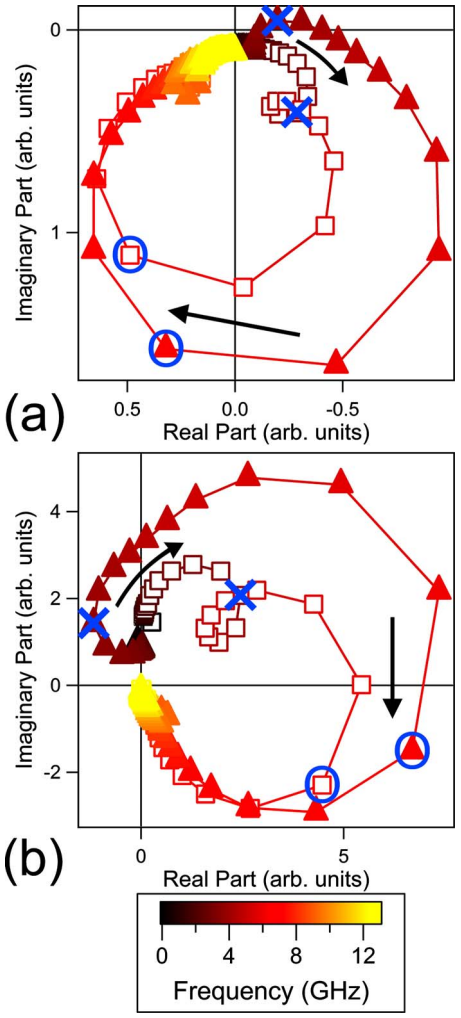

FIG. 4. (Color online) Argand diagrams showing the FFT response from the numerical simulations of the (a) m_z and (b) m_r components of magnetization in the PL (▲) and FL (□) for H_{eb} =104 Oe and H_{IEC}=+62.5 Oe. Two modes are apparent at 3.5 (×) and 6.0 GHz (◯), and the phase relation and relative amplitude of the two modes is consistent with the analytical result seen in Figs. 3(b) and 3(c).

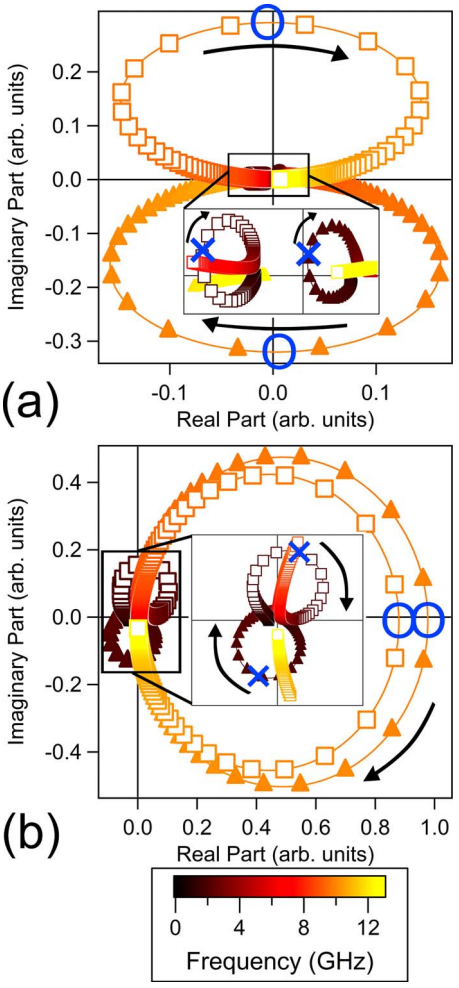

FIG. 5. (Color online) Argand diagrams showing the FFT response of the (a) m_z and (b) m_r components of magnetization in the PL (▲) and FL (□) calculated from the analytical model (H_{eb} =100 Oe and H_{IEC}=−60 Oe). At the low-frequency mode at 2.0 GHz (×) (magnified in insets) the m_z components in the FL and PL are in phase, and the m_r components are 180° out of phase. The opposite phase relation is observed at the higher frequency mode seen at 9.8 GHz (◯).

functions. The results of the numerical model also include additional high-frequency behavior in the range of 8–10 GHz resulting from higher-order modes, which were not included in the simple analytical model. These modes have been discussed previously for isolated and exchange-biased disks[9,11,26] and will not be discussed in further detail here.

B. Dynamic response for negative interlayer exchange coupling

Similar Argand diagrams were generated for an IEC field of −60 Oe for both the m_r and m_z components of magnetization using the analytical model, and the results are shown in Figs. 5(a) and 5(b). Similar to the results for the positive IEC, two circles are found representing the low and high-frequency modes of the system at 2.0 and 9.8 GHz. As was the case for positive IEC, the high-frequency mode has larger amplitude than the low-frequency mode and the response of the PL components of magnetization has larger amplitude than that of the FL for the high-frequency mode, whereas the converse is true for the low-frequency mode. At the high-frequency mode, the radial components of magnetization in the PL and FL are in phase, while the z components are 180° out of phase. At both modes, the radial and z components within each layer are approximately 90° out of phase. However, the phase relation between the z components of magnetization in the two layers is more complicated due to a competition between exchange bias and IEC in the restoring torque equation at the low-frequency mode and will be discussed later.

Corresponding numerical simulations using an IEC field of −62.5 Oe showed much more complicated behavior (results not shown). The FFTs calculated from these simulations routinely showed a clear low-frequency mode in which the z components of magnetization move in phase, while the m_r components moved out of phase. However, there was little

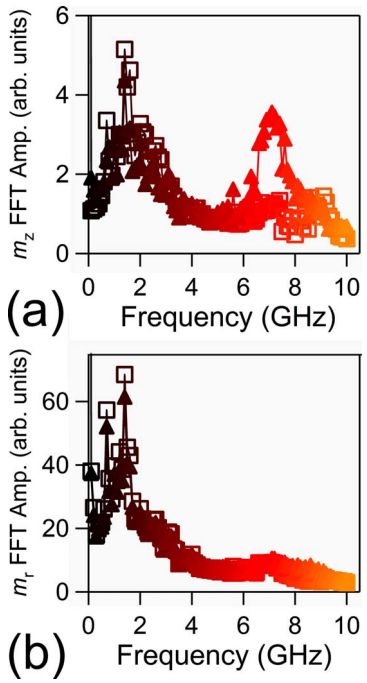

FIG. 6. (Color online) FFT response of the (a) m_z and (b) m_r components of magnetization to a pumped ac magnetic field at various frequencies in the PL (▲) and FL (□), calculated from numerical simulations (H_{eb}=104 Oe, H_{IEC}=−62.5 Oe). In the figure is plotted the sum of the FFTs at all pump frequencies with the specific pump frequency response subtracted. The plot shows a clear low-frequency response (1.4 GHz) and a possible high-frequency response (~7 GHz).

definitive evidence of the expected high-frequency branch behavior. The following additional numerical simulations were performed to explain this discrepancy.

1. Pumped field numerical simulations

One possible reason for not observing a high-frequency mode could be that such a mode is strongly damped for negative IEC. In the numerical simulations in which a field pulse was applied to the system, a strongly damped response would be difficult to discern but could be more easily detected if the system was driven at the resonance frequency of the mode. Therefore, a series of simulations were performed with an ac pumping field. The simulations covered a range of pumping frequencies with a fixed frequency for each simulation. While no clear resonance was observed at any frequency, for each frequency, transient responses at about 1.4 and 7 GHz were observed in the FFTs of the average magnetization components. In order to illustrate these transients more clearly, a compound FFT was generated by adding the individual FFTs from different pumping frequencies together, and subtracting the response at each specific pumping frequency. This allows the rather weak transient responses to be visualized. These are shown in Fig. 6 for both the radial and z components of magnetization. The low-frequency response is seen as a broad peak due to the presence of several higher-order modes within this frequency range. For the high-frequency response, a clear peak is visible at 7 GHz in the plot of m_z for the pinned layer, but the response of m_z in the free layer and m_r in both layers is much more subtle at this frequency. This of course does not prove the existence of eigenmodes at these frequencies, but does give an indication that there are resonances at them.

2. Effect of vortex core-core interactions

It is possible that vortex core-core interactions, included in the numerical simulations but omitted from the analytical model, are responsible for the difference between the responses observed for the analytical and numerical models for negative IEC. These interactions might be responsible for coupling the high-frequency mode to other dynamics, such as spin waves or core dynamics, effectively damping out the high-frequency eigenmode. In order to investigate this possibility, numerical simulations were performed in which the magnetization of each layer was removed from a circular region of diameter 40 nm at the center. In this way, the layers kept their vortex configuration but the vortex cores were removed. However, clear evidence for the eigenmodes was not seen either for pulsed or driven excitations of the system. In contrast, a comparable simulation with positive IEC reproduced the same dynamic response with and without the circular region removed. Therefore, vortex core-core interactions were not responsible for making the high-frequency mode unobservable for negative IEC.

3. Effect of decreasing the magnetization density M_S

The negative values of IEC could shift the frequencies of the spin-wave sector such that the high-frequency eigenmode was immersed in a spin-wave continuum and therefore strongly damped. In order to further clarify the behavior of the system with a negative IEC, analytical and numerical simulations were performed on a system with a magnetization density (M_s) of only 300 emu/cm^3. This was done in order to shift the upper branch behavior to a lower frequency, away from the expected short-wavelength spin-wave frequencies. The strength of the exchange-bias field H_{eb} was maintained at its standard strength by appropriately adjusting the exchange-bias energy density ε_{eb}. The results from the analytical model calculations using the decreased value of M_S are plotted on Argand diagrams in Figs. 7(a) and 7(b) for the m_z and m_r components of magnetization. The two distinct (1,0) modes are readily apparent and show similar behavior as before, but at lower frequencies (1.3 and 4.2 GHz for the lower and upper branches, respectively, compared to 2.0 and 9.8 GHz for M_S=800 emu/cm^3). The results of the similar numerical simulation are plotted in Fig. 8. In this simulation the two expected modes are identifiable at 1.1 and 3.8 GHz, and show good agreement with the analytical result for both the frequency of the modes and also the relative phases of the response in both m_r and m_z. However, it is interesting to note that the amplitude of the response of the high-frequency mode is still much lower in the numerical simulation than is expected from the analytical model. This suggests that the high-frequency mode continues to be quickly damped. Inspection of the symmetry of the two modes at 1.1 and 3.8 GHz found in the numerical simulation confirms that they

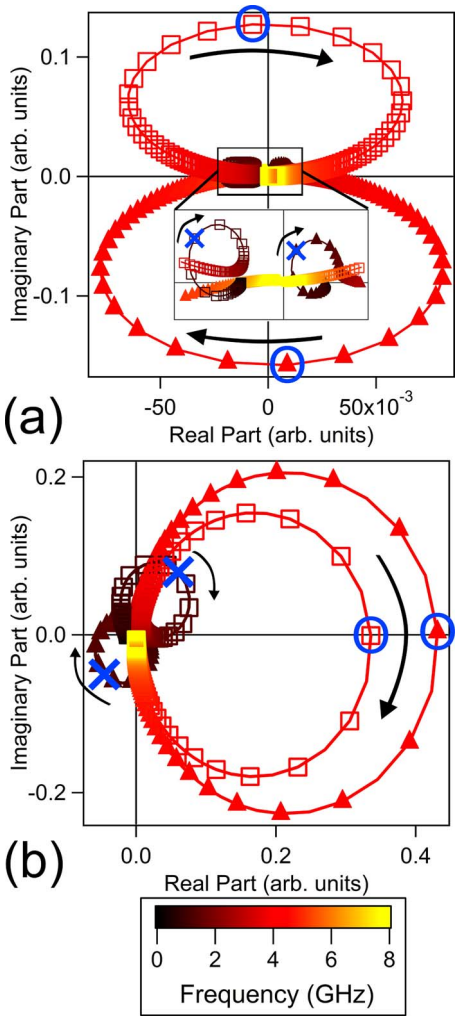

FIG. 7. (Color online) Argand diagrams showing the FFT response of the (a) m_z and (b) m_r components of magnetization in the PL (▲) and FL (□) calculated from the analytical model: $H_{eb}=100$ Oe, $H_{IEC}=-60$ Oe, but a reduced saturation magnetization of $M_S=300$ emu/cm^3. The qualitative phase relations and relative amplitude of the modes are the same as for higher M_S, but mode frequencies have been redshifted to 1.3 (×) and 4.2 GHz (◯) for the lower and upper branches, respectively.

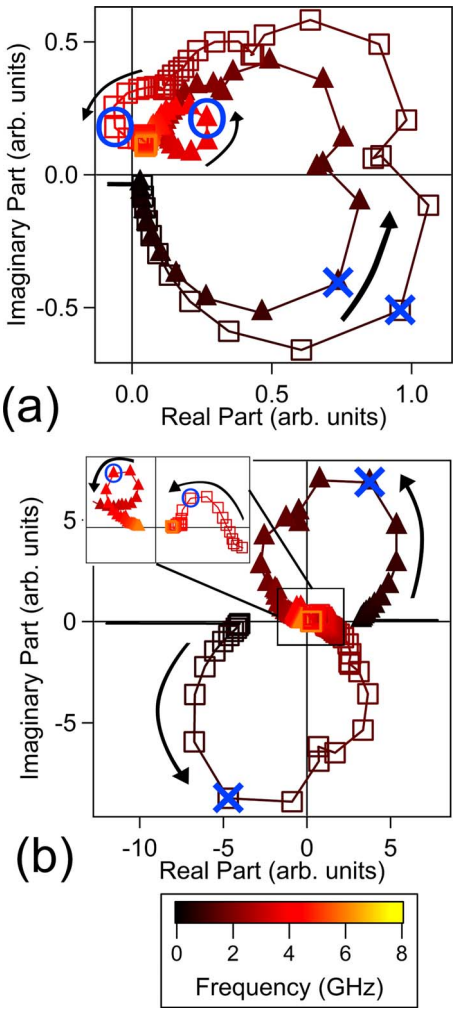

FIG. 8. (Color online) Argand diagrams showing the FFT response calculated from the numerical simulations of the (a) m_z and (b) m_r components of magnetization in the PL (▲) and FL (□): $H_{eb}=104$ Oe, $H_{IEC}=-62.5$ Oe and $M_S=300$ emu/cm^3. Both low- and high-frequency modes (1.1 (×) and 3.8 GHz (◯), respectively) are now apparent, and have the expected phase relationship seen in the analytical model for negative values of IEC. However, the high-frequency mode is severely damped, in particular in the m_r response [see inset (b)].

are in fact (1,0) modes, which was previously difficult to conclude for the upper branch response with $M_S=800$ emu/cm^3.

C. Restoring torque: balancing H_{eb} against IEC

As could be seen from Fig. 5, the phase relation between the z components of magnetization in the FL and PL for negative IEC is complicated at the low-frequency mode. In order to investigate this further, the relative effects of the restoring forces exerted on the magnetic moments in the two layers by the IEC field and by the exchange-bias field were investigated. The nature of the modes can be obtained by considering the magnetostatic fields—at the high-frequency mode, the radial components of the PL and FL magnetization are in phase, resulting in a large magnetostatic field in the radial direction and a mode frequency almost independent of IEC and only weakly dependent on exchange bias. At the lower-frequency mode, the radial components of the PL and FL magnetizations are out of phase and the magnetostatic fields cancel to lowest order, resulting in a lower frequency and a dispersion dominated by IEC and exchange bias. By assuming that $\delta\hat{m}_{PL}=\delta m_{PL}M_S\hat{r}$ and $\delta\hat{m}_{FL}=-\delta m_{FL}M_S\hat{r}$, Eqs. (8) and (9) show that the torques exerted on the magnetization in the FL and PL, respectively, for positive IEC, are

$$\boldsymbol{\tau}_{FL}=-(M_S\hat{\varphi}\times H_{IEC}\hat{r})\delta m_{PL}=M_S H_{IEC}\delta m_{PL}\hat{z}, \tag{8}$$

$$\begin{aligned}\boldsymbol{\tau}_{PL}&=-[M_S\hat{\varphi}\times(H_{IEC}\delta m_{FL}\hat{r})]-[M_S\delta m_{PL}\hat{r}\times H_{eb}\hat{\varphi}]\\&=-(M_S H_{IEC}\delta m_{FL}+M_S H_{eb}\delta m_{PL})\hat{z}.\end{aligned} \tag{9}$$

As can be seen, the contributions from H_{IEC} and H_{eb} to the torque on the PL magnetization act in the same direction, and

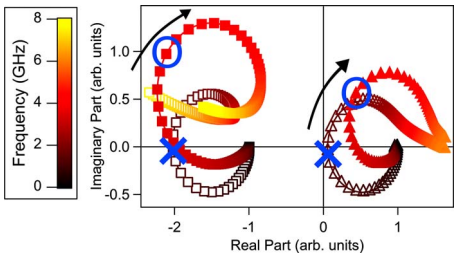

FIG. 9. (Color online) Argand diagrams from the analytical model showing the FFT of the low-frequency m_z response for weak and strong values of H_{eb} with $H_{IEC}=-60$ Oe and $M_S=800$ emu/cm^3: PL $H_{eb}=50$ Oe (△), FL $H_{eb}=50$ Oe (□), PL $H_{eb}=400$ Oe (▲), FL $H_{eb}=400$ Oe (■). The resonant frequencies are 1.4 (×) and 3.8 GHz (◯) for H_{eb} of 50 and 400 Oe, respectively. In addition to changing the resonant frequency of the eigenmodes, altering the strength of H_{eb} changes the energy balance between exchange bias and IEC in the restoring torque equations, and shifts the relative phase of the m_z response in the low-frequency mode.

therefore the relative phase of m_z between the pinned layer and free layer remains fixed. For negative IEC, however, the situation is more complicated, as can be seen from Eqs. (10) and (11),

$$\boldsymbol{\tau}_{FL} = -\left[-M_S\hat{\varphi} \times (-H_{IEC}\hat{r})\,\delta m_{PL}\right] = M_S H_{IEC}\delta m_{PL}\hat{z}, \tag{10}$$

$$\boldsymbol{\tau}_{PL} = -\{M_S\hat{\varphi} \times [-H_{IEC}\delta m_{FL}(-\hat{r})]\} - (M_S\delta m_{PL}\hat{r} \times H_{eb}\hat{\varphi})$$
$$= (M_S H_{IEC}\delta m_{FL} - M_S H_{eb}\delta m_{PL})\hat{z} \tag{11}$$

In this case, the contributions from IEC and from exchange bias to the torque on the pinned layer magnetization, $\boldsymbol{\tau}_{PL}$, act in opposite directions, such that the sign of $\boldsymbol{\tau}_{PL}$ will depend on the relative strengths of the IEC and exchange bias. This will then also affect the relative phase of the z components of magnetization in the FL and PL. Two examples of this for the low-frequency mode are shown on the Argand diagram in Fig. 9. In both cases the value of H_{IEC} is −60 Oe. The FL response is to the left of the axis and the PL response is to the right. The two data sets shown are for $H_{eb}=50$ Oe and 400 Oe. As can be seen, for $H_{eb}=50$ Oe, the peak positions for both FL and PL response lie on the real axis, however for $H_{eb}=400$ Oe, this is not the case. Both the PL and the FL response have shifted vertically up the imaginary axis, with the shift being greater for the FL response than for the PL response. In addition the PL response has shifted along the positive real axis. These changes lead to a difference in the relative phase of m_z for the two layers. Furthermore, as the magnetostatic fields nearly cancel at the lower-frequency mode, the PL response is controlled by exchange bias and IEC, while the FL response is controlled only by IEC, in addition to the relatively weak magnetostatic fields. Therefore, the FL response has a larger amplitude at this mode, and a small change in exchange bias results in a larger change in the FL response than in the PL. A final point to note is that increasing the strength of H_{eb} shifts the mode frequency to a higher value, in this case from 1.4 GHz for $H_{eb}=50$ Oe to 3.8 GHz for $H_{eb}=400$ Oe. The upper branch experiences a similar shift from 9.7 to 10.7 GHz. These shifts are in good agreement with previous studies of the effect of H_{eb} on resonant mode frequencies in exchange-biased magnetic vortices.[5,11] This demonstrates that the strength of H_{eb}, in addition to and independent of IEC, can be used to alter the frequency response of the system.

IV. DISCUSSION

For the magnetic heterostructure under consideration, two stable magnetic configurations were identified by micromagnetic simulations in which each ferromagnetic layer has a centered vortex as its stable magnetic configuration. For positive values of interlayer exchange coupling, the chirality of the two vortices was found to be parallel, while for negative IEC the chirality was antiparallel. This is in good agreement with previous work by Buchanan *et al.*[13] Single domain states can also be expected to arise from this multilayer structure, but were not seen in this study due to the choices of materials and dimensions.

Magnetostatic and IEC interactions couple the modes of the individual ferromagnetic layers. In the present work, the coupled (1,0) modes, which are split into two separate branches as a result of the coupling, have been considered. A simple analytical model, in which the restoring torques arose because of IEC, exchange bias, and approximate magnetostatic fields based on a nodeless trial function for the individual (1,0) modes, was compared with micromagnetic simulations. By comparing the results from the two models it is possible to determine which interactions control the dispersion relations and phase relations of the coupled (1,0) branches.

For positive IEC, the agreement between the analytical and numerical models is very good. The lower branch of the coupled (1,0) modes has a positive dispersion as a function of the IEC, while the upper branch is rather flat. The agreement between the two models confirms that exchange bias, IEC, and the magnetostatic field from the near-uniform modes control the frequencies. The magnetostatic fields are primarily in the radial direction. In the lower branch, the radial components of magnetization in the PL and FL are out of phase with the consequence that the magnetostatic fields from the PL and FL nearly cancel each other in each layer. The restoring torque is then almost exclusively a result of IEC and exchange bias (on the PL). With the radial components of magnetization out of phase, the restoring torques increase with increasing IEC, with increasing frequency as a consequence. The fact that the magnetostatic fields cancel also leads to the agreement between the numerical and analytical results being very good—the main approximation in the analytical model is the shape of the magnetostatic fields, and they do not affect the frequency of these modes.

In the upper branch the radial components of magnetization in the PL and FL move in phase for positive IEC. Therefore, the dispersion of this branch is controlled by the magnetostatic fields, while the IEC plays an insignificant role (an increase in frequency with IEC is a result of the fact that the z components of magnetization in the two layers are 180° out

of phase). Here, the shape of the trial function used in the analytical model clearly matters and the analytical model, being a variational model, overestimates the frequencies of this branch, which is consistent with the results of similar calculations on bilayer vortices.[11]

For negative IEC, there are significant discrepancies between the results of the numerical and analytical models for the approximate Py parameters used here. The possibility that these discrepancies result from vortex core-core interactions was ruled out by performing numerical simulations in which the vortex cores had been removed. As stated earlier, the analytical model is based on a linear response to restoring torques only from exchange bias, IEC, and magnetostatic fields from the simple nodeless trial functions for the magnetization response. This model does not contain spin-wave modes driven primarily by intralayer ferromagnetic exchange, while the numerical simulations do. This suggests that for negative IEC, the spin-wave sector of the spectrum is significantly redshifted to immerse the upper branch of the coupled (1,0) mode in the spin-wave sector. As a consequence, the high frequency coupled (1,0) modes would be heavily damped because of coupling to spin waves, and thus rendered nearly unobservable. This suggestion was supported by numerical simulations in which the magnetization density was reduced, while the IEC and exchange-bias fields were kept constant. This had the effect of reducing the magnetostatic field from the nodeless coupled (1,0) modes, with a resulting large separation in frequency between these modes and the intralayer exchange-driven spin waves. As a consequence, the coupled (1,0) modes were less damped and therefore observable in the numerical simulations.

It is important to note that a redshift of the spin-wave spectrum cannot be obtained perturbatively from linear-response theory. This suggests that nonlinear coupling between magnetostatic fields, IEC, and exchange fields are important in mixing the spin waves with the coupled (1,0) modes. It is an interesting observation that for zero IEC, the numerical and analytical models agree well, and the response is obtained by continuation from the positive-IEC branches. However, even for very small but negative IEC, the large discrepancies between the numerical and analytical models appear (for Py parameters). This suggests that negative IEC acts as a singular perturbation on the nonlinear coupling between magnetostatic fields and exchange.

Higher-order eigenmodes can also be seen within the results of the numerical simulations for both positive and negative IEC. For example, the FFT spectra with positive IEC show clear peaks for the (2,0) and (3,0) modes in the upper branch at frequencies of 9.5 and 11.5 GHz, respectively. However, these peaks are difficult to visualize in the Argand diagram shown in Fig. 4 since the amplitudes are nearly an order of magnitude smaller than the (1,0) mode. In contrast, the (2,0) mode of the lower branch for negative IEC is quite visible in Fig. 8 at 1.5 GHz since it has nearly the same amplitude as the (1,0) mode at 1.1 GHz

V. CONCLUSIONS

In summary, the magnetization dynamics in a disk-shaped, magnetically coupled multilayer structure consisting of two Py layers, each in a vortex configuration and separated by a nonmagnetic spacer, in response to a magnetic field pulse applied normal to the plane of the disk have been studied using an analytical model and numerical micromagnetic simulations. The sign of the interlayer exchange coupling between the two Py layers led to either parallel or antiparallel vortex chiralities in the remanent state. For both positive and negative IEC, both analytical and numerical results showed a two-branched frequency response for the lowest order circularly symmetric (1,0) eigenmode. For positive interlayer exchange coupling, the upper and lower branches are determined by magnetostatic fields and IEC, respectively. This means that these mode frequencies and, to some extent, the difference between them, can be controlled in applications by materials selections for the ferromagnetic layers and the spacer layer, as well as by the thickness of the spacer layer. For negative IEC, the spectrum is much more complicated because of interactions between magnetostatic fields, IEC, and ferromagnetic exchange, leading to a wider range of parameters that can be used to control the response of the system and thus "tune" it for particular technological applications.

ACKNOWLEDGMENTS

A.K.P.L. and D.K.S. acknowledge UChicago Argonne, LLC, operator of the Argonne National Laboratory ("Argonne"). Argonne, a U.S. Department of Energy Office of Science Laboratory, is operated under Contract No. DE-AC02-06CH11357.

*danielschreiber2008@u.northwestern.edu

[1] R. P. Cowburn, D. K. Koltsov, A. O. Adeyeye, M. E. Welland, and D. M. Tricker, Phys. Rev. Lett. **83**, 1042 (1999).
[2] T. Shinjo, T. Okuno, R. Hassdorf, K. Shigeto, and T. Ono, Science **289**, 930 (2000).
[3] M. Tanase, A. K. Petford-Long, O. Heinonen, K. S. Buchanan, J. Sort, and J. Nogues, Phys. Rev. B **79**, 014436 (2009).
[4] K. Y. Guslienko, J. Nanosci. Nanotechnol. **8**, 2745 (2008).
[5] K. S. Buchanan, A. Hoffmann, V. Novosad, and S. D. Bader, J. Appl. Phys. **103**, 07B102 (2008).
[6] K. Y. Guslienko, X. F. Han, D. J. Keavney, R. Divan, and S. D. Bader, Phys. Rev. Lett. **96**, 067205 (2006).
[7] B. A. Ivanov and C. E. Zaspel, J. Appl. Phys. **95**, 7444 (2004).
[8] R. Zivieri and F. Nizzoli, Phys. Rev. B **71**, 014411 (2005).
[9] M. Buess, T. P. J. Knowles, R. Hollinger, T. Haug, U. Krey, D. Weiss, D. Pescia, M. R. Scheinfein, and C. H. Back, Phys. Rev. B **71**, 104415 (2005).
[10] I. Neudecker, K. Perzlmaier, F. Hoffmann, G. Woltersdorf, M. Buess, D. Weiss, and C. H. Back, Phys. Rev. B **73**, 134426 (2006).

[11] O. G. Heinonen, D. K. Schreiber, and A. K. Petford-Long, Phys. Rev. B **76**, 144407 (2007).
[12] J. G. Zhu, Y. F. Zheng, and G. A. Prinz, J. Appl. Phys. **87**, 6668 (2000).
[13] K. S. Buchanan, K. Y. Guslienko, A. Doran, A. Scholl, S. D. Bader, and V. Novosad, Phys. Rev. B **72**, 134415 (2005).
[14] K. Y. Guslienko, K. S. Buchanan, S. D. Bader, and V. Novosad, Appl. Phys. Lett. **86**, 223112 (2005).
[15] F. Montoncello, L. Giovannini, and F. Nizzoli, in *Proceedings of the 53rd Annual Conference on Magnetism and Magnetic Materials, Austin, Texas, 2009*; J. Appl. Phys. **105**, 07E304 (2009).
[16] G. Binasch, P. Grunberg, F. Saurenbach, and W. Zinn, Phys. Rev. B **39**, 4828 (1989).
[17] M. N. Baibich, J. M. Broto, A. Fert, F. Nguyen Van Dau, F. Petroff, P. Etienne, G. Creuzet, A. Friederich, and J. Chazelas, Phys. Rev. Lett. **61**, 2472 (1988).
[18] J. L. Leal and M. H. Kryder, J. Appl. Phys. **83**, 3720 (1998).
[19] E. Popova, N. Keller, F. Gendron, C. Tiusan, A. Schuhl, and N. A. Lesnik, Appl. Phys. Lett. **91**, 112504 (2007).
[20] T. Katayama, S. Yuasa, J. Velev, M. Y. Zhuravlev, S. S. Jaswal, and E. Y. Tsymbal, Appl. Phys. Lett. **89**, 112503 (2006).
[21] J. Sort, K. S. Buchanan, V. Novosad, A. Hoffmann, G. Salazar-Alvarez, A. Bollero, M. D. Baro, B. Dieny, and J. Nogues, Phys. Rev. Lett. **97**, 067201 (2006).
[22] L. Neel, C. R. Acad. Sci. **255**, 1676 (1962).
[23] S. S. P. Parkin, Phys. Rev. Lett. **67**, 3598 (1991).
[24] W. H. Press, *Numerical Recipes in FORTRAN 90: The Art of Parallel Scientific Computing* (Cambridge University Press, Cambridge, England, 1996).
[25] M. Buess, R. Hollinger, T. Haug, K. Perzlmaier, U. Krey, D. Pescia, M. R. Scheinfein, D. Weiss, and C. H. Back, Phys. Rev. Lett. **93**, 077207 (2004).
[26] K. Y. Guslienko and A. N. Slavin, J. Appl. Phys. **87**, 6337 (2000).